



POLİTEKNİK DERGİSİ

*JOURNAL of POLYTECHNIC*

ISSN: 1302-0900 (PRINT), ISSN: 2147-9429 (ONLINE)

URL: <http://dergipark.org.tr/politeknik>



# Deep learning-based classification of breast tumors using raw microwave imaging data

*Ham mikrodalga görüntüleme verilerini kullanarak meme tümörlerinin derin öğrenme tabanlı sınıflandırılması*

*Author(s): Mustafa Berkan BİÇER<sup>1</sup>, Uğur ELİİYİ<sup>2</sup>, Deniz TÜRSEL ELİİYİ<sup>3</sup>*

*ORCID<sup>1</sup>: 0000-0003-3278-6071*

*ORCID<sup>2</sup>: 0000-0002-5584-891X*

*ORCID<sup>3</sup>: 0000-0001-7693-3980*

**To cite to this article:** Bicer M. B., Eliyi U. and Tursel-Eliyi D., “Deep learning-based classification of breast tumors using raw microwave imaging data”, *Journal of Polytechnic*, \*(\*) : \*, (\*).

**Bu makaleye şu şekilde atıfta bulunabilirsiniz:** Bicer M. B., Eliyi U. ve Tursel-Eliyi D., “Deep learning-based classification of breast tumors using raw microwave imaging data”, *Politeknik Dergisi*, \*(\*) : \*, (\*).

**To link to this article:** <http://dergipark.org.tr/politeknik/archive>

**DOI:** 10.2339/politeknik.1056839

# Deep Learning-based Classification of Breast Tumors using Raw Microwave Imaging Data

## Highlights

- ❖ Microwave imaging (MWI), combined with a novel convolutional neural network (CNN) model, offers a cost-effective and efficient approach for detecting and classifying breast tumor scatterers.
- ❖ The proposed CNN model, trained and tested on MWI simulation data, achieves exceptional accuracy rates of 99.61% and 99.75% for tumor detection and classification, respectively.
- ❖ The integration of microwave imaging and deep learning techniques provides a cutting-edge computer-aided diagnosis (CAD) solution for breast cancer, enabling swift and precise interpretation of measurements to support early-stage treatment decisions.

## Graphical Abstract

This study proposes a novel convolutional neural network (CNN) model for the detection and classification of tumor scatterers in microwave imaging (MWI) simulation data, aiming to overcome the limitations of existing breast screening techniques by leveraging the potential of MWI as a cost-effective and non-ionizing imaging modality.

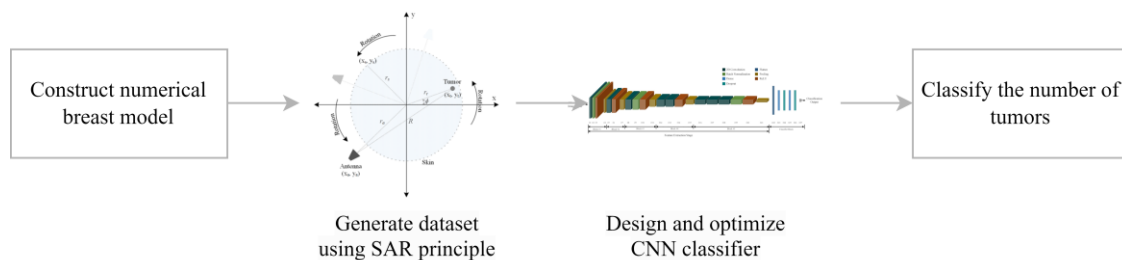


**Figure.** Data generation and classification procedure using CNN model

## Aim

The aim of this study is to propose a novel CNN model for detecting and classifying tumor scatterers in MWI simulation data.

## Design & Methodology

The study involved the development of a comprehensive dataset and the construction of a multi-layered CNN model with five convolutional blocks.

## Originality

The originality of this research lies in the development of a CNN model specifically tailored for the analysis of MWI simulation data.

## Findings

The findings demonstrate the effectiveness of the proposed CNN model in accurately detecting and classifying tumor scatterers in MWI simulation data.

## Conclusion

In conclusion, this study presents a novel CNN model for the detection and classification of tumor scatterers in MWI simulation data, highlighting the potential of MWI as a valuable imaging modality for breast cancer detection.

## Declaration of Ethical Standards

The author(s) of this article declare that the materials and methods used in this study do not require ethical committee permission and/or legal-special permission.

# Deep Learning-based Classification of Breast Tumors using Raw Microwave Imaging Data

*Araştırma Makalesi / Research Article*

Mustafa Berkan BİÇER<sup>1\*</sup>, Uğur ELİİYİ<sup>2</sup>, Deniz TÜRSEL ELİİYİ<sup>3</sup>

<sup>1</sup>Engineering Faculty, Electrical and Electronics Engineering Department, Tarsus University, Türkiye

<sup>2</sup>Economics and Administrative Sciences Faculty, Business Department, Izmir Bakircay University, Türkiye

<sup>3</sup>Engineering and Architecture Faculty, Industrial Engineering Department, Izmir Bakircay University, Türkiye

(Geliş/Received : 12.01.2022 ; Kabul/Accepted : 30.05.2023 ; Erken Görünüm/Early View : 14.06.2023)

## ABSTRACT

Breast cancer is the leading type of malignant neoplasm disease among women worldwide. Breast screening makes extensive use of powerful techniques such as x-ray mammography, magnetic resonance imaging, and ultrasonography. While these technologies have numerous benefits, certain drawbacks such as the use of low-energy ionizing x-rays, a lack of specificity for malignant tissues, and cost, have motivated researchers to investigate novel imaging and detection modalities. Microwave imaging (MWI) has been extensively studied due to its low-cost structure and ability to perform measurements using non-ionizing electromagnetic waves. This study proposes a novel convolutional neural network (CNN) model for detecting and classifying tumor scatterers in MWI simulation data. To accomplish this, 10001 different numerical breast models with tumor scatterers of varying numbers and positions were developed, and the simulation results were derived using the synthetic aperture radar (SAR) technique. The presented CNN structure was trained using 8000 pieces of simulation data, and the remaining data were used for testing, achieving accuracy rates of 99.61% and 99.75%, respectively. The proposed model is compared to three state-of-the-art models on the same dataset in terms of classification performance. The results demonstrate that the proposed model effectively performs effectively well in detecting and classifying tumor scatterers.

**Keywords:** Breast cancer, classification, convolutional neural networks, deep learning, microwave imaging.

## Ham Mikrodalga Görüntüleme Verilerini Kullanarak Meme Tümörlerinin Derin Öğrenme Tabanlı Sınıflandırılması

### ÖZ

Meme kanseri, dünya genelinde kadınlar arasında en yaygın türdeki kötü huylu tümör hastalığıdır. Meme taraması, x-ışını mamografisi, manyetik rezonans görüntüleme ve ultrasonografi gibi güçlü teknikleri yoğun bir şekilde kullanır. Bu teknolojilerin birçok faydası olsa da, düşük enerjili iyonlaştırıcı x-ışınlarının kullanımı, kötü huylu dokular için yetersizlik ve maliyet gibi bazı dezavantajlar, araştırmacıları yeni görüntüleme ve tespit yöntemlerini araştırmaya teşvik etmiştir. Mikrodalga görüntüleme (MDG), düşük maliyetli yapısı ve iyonlaştırıcı olmayan elektromanyetik dalgalar kullanarak ölçümler yapabileceği nedeniyle yoğun bir şekilde araştırılmaktadır. Bu çalışma, MDG simülasyon verilerinde tümör saçıklarını tespit etmek ve sınıflandırmak için yeni bir ESA modeli önermektedir. Bunun için farklı sayı ve pozisyonlar tümör saçıklarına sahip 10001 farklı sayısal meme modeli geliştirilmiştir ve sentetik açıklıklı radar (SAR) tekniği kullanılarak simülasyon sonuçları elde edilmiştir. Sunulan ESA yapısı, 8000 adet simülasyon verisi kullanılarak eğitilmiş ve kalan veriler test için kullanılarak sırasıyla %99.61 ve %99.75 doğruluk oranlarına ulaşılmıştır. Önerilen model, sınıflandırma performansı açısından aynı veri kümesi üzerinde üç farklı güncel modelle karşılaştırılmıştır. Sonuçlar, önerilen modelin tümör saçıklarını tespit edip sınıflandırmada etkili bir şekilde çalıştığını göstermektedir.

**Anahtar Kelimeler:** Meme kanseri, sınıflandırma, evrişimli sinir ağları, derin öğrenme, mikrodalga görüntüleme.

### 1. INTRODUCTION

Breast cancer is a slow-growing type of cancer that can lead to fatal outcomes when it metastasizes to other tissues and organs, making early diagnosis and treatment of breast tumors crucial [1], [2]. Breast screening currently relies heavily on primary modalities such as x-ray mammography, ultrasonography imaging (USI), and

magnetic resonance imaging (MRI) [2], [3]. Since x-ray mammography utilizes high-frequency ionizing waves at low energy levels, it cannot be used repetitively on patients. Additionally, the requirement to compress the patient's breast for better imaging and the recommendation to use it for women over the age of 40 (since the breast structures typically contain adipose tissue) are among the drawbacks of the x-ray. While MRI can be used to overcome many of the drawbacks of mammography, it does have some adverse circumstances, including discomfort and prolonged

\*Sorumlu yazar (Corresponding Author)  
e-posta : mberkanbicer@tarsus.edu.tr

measurement time, limited mobility, a high cost, and the potential for unnecessary biopsies. Although it may appear to be an alternative to these methods, the USI, which employs sound waves to image at frequencies beyond the hearing range of the human ear, can only detect the presence of neoplasms within the breast structure and requires additional modalities such as x-ray mammography, MRI, or biopsy for more accurate results. Microwave imaging (MWI), which is widely used in underground, through-the-wall, under-rubble, and tree-interior imaging, as well as hidden object identification and border surveillance in the defense applications, has tremendous potential in the imaging and treatment of diseases. Due to its low cost, portability, low energy level, and low spectral range, MWI overcomes the disadvantages of traditional techniques and has gained attention from researchers studying early-stage breast cancer detection [4]–[19].

The most critical procedure in computer-aided diagnosis (CAD) is the classification of medical images. While recent advancements in medical image classification techniques with machine learning tools assist doctors and specialists, it provides convenience in monitoring and managing disease progression. Rapid and accurate interpretation of the measurements enables rapid and precise treatment decisions to be made during the early stages. Furthermore, knowing the number of tumors in the raw measurement data prior to producing the resultant image assists in appropriately interpreting the image.

In the literature, numerous researches on the classification of breast tissues utilizing mammography, MRI, USI, and MWI images have been studied [20]–[27]. Tan et al. [21] proposed a study on employing support vector machines (SVM) to extract features and classify mammograms using the sequential forward shifting selection (SFFS) technique. Using region of interest (ROI) data, the classification of 600 benign and 600 malignant mammographic images is performed, and an area under curve (AUC) value of  $0.805 \pm 0.012$  is achieved [21]. Zennaro et al. proposed a method for binary tissue classification using mammograms based on semi-supervised support vector machine (S3VM) [20]. In their study, an accuracy of 92% was achieved using a feature extraction method based on genetic algorithm [20]. Yin et al. [23] presented a statistical classifier for the images obtained by the dynamic contrast-enhanced magnetic resonance imaging (DCE-MRI) method. In the time-intensity curve (TIC) categorization using data with 85 malignant and 71 benign breast lesions, sensitivity, specificity, and accuracy values were 83.5%, 80.3%, and 82.1%, respectively [23]. Abdel-Nasser et al. [25] demonstrated a random forest classifier model for classifying USI that contained 31 malignant and 28 benign cases with an AUC of 0.99. Conceição et al. [27] extracted the features from the radar target signature (RTS) data using principal component analysis (PCA) and classified the extracted features based on their size and shape using a novel SVM-based classification approach. They classified the size of 352 breast tumors

with an accuracy of 94.89% and 86.93% for coarse and fine groups, respectively [27].

The focus of this research is to present a novel convolutional neural network (CNN) model for determining the number of breast tumors in a data set using the numerical breast model. A numerical breast model was built to accomplish this, and backscattered electric field data for 10001 distinct scenarios were computed using the monostatic synthetic aperture radar (SAR) approach. Following that, a CNN model with five convolutional blocks was constructed. The proposed model was trained employing 80% of the data and tested on 20% of the data to demonstrate the performance. The performance of the proposed model was also compared to that of Xception [28], ResNet152V2 [29], and DenseNet201 [30] models. Additionally, five-fold cross-validation results for the abovementioned models are presented in comparison. The results demonstrate that the proposed CNN model classifies raw electric field data acquired via MWI successfully.

## 2. GENERATION OF DATA FOR CLASSIFICATION

The data set utilized in the deep learning model for classification was constructed using calculations based on the synthetic aperture radar (SAR) approach. Monostatic SAR is a technique that involves rotating the transceiver antenna in a circular path around an object at predetermined angles and acquiring the scattering electric field. In SAR, the object to be imaged remains stationary and concentrically aligned with the transceiver antenna [31]. Figure 1 depicts the numerical setup based on the monostatic SAR concept, which includes transceiver antennas and the breast model to generate breast imaging data.

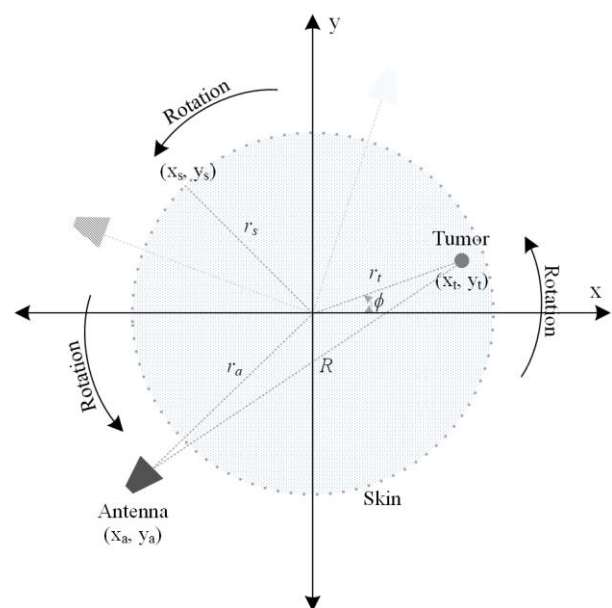


**Figure 1.** Configuration for the generation of electric field data using the SAR approach

In the numerical setup illustrated in Figure 1, a monostatic measurement setup consisting of a skin structure formed by  $n_s$  discrete perfect point scatterers, a tumor formed by  $n_t$  discrete scatterers, and transceiver antennas positioned concentrically with the skin may be observed. The electric field reflected by the skin scatterers was assumed to have an amplitude twenty times that of the tumor scatterers. The skin radius was  $r_s$ , the distance between the antenna and the center was determined as  $r_a > r_s + D_{GAP}$ , and the position of the tumor was randomly chosen as  $0 \leq r_t < 2r_s$ .  $D_{GAP}$  denotes the space between the antenna and the surface of the skin. The antenna rotates in a counterclockwise direction at an angle of  $0 \leq \phi \leq 2\pi$ . The radiation pattern of the antenna is considered to cover the entire imaging region. In the SAR principle, the scattered electric field from each discrete scatterer for any angle and frequency value is calculated according to Equation (1) [31].

$$\mathbf{E}_s(f, \phi) = A_0 e^{-j\left(\frac{4\pi f}{v}\right)R(\phi)} \quad (1)$$

In Equation (1),  $A_0$ ,  $f$ ,  $v$ ,  $R$ , and  $\phi$  parameters denote the amplitude of the scattered electric field, the frequency, the velocity of the electromagnetic wave within a medium, the Euclidean distance function, and the angle formed by the antenna with respect to the x-axis, respectively. Equation (2) defined the Euclidean function denoted by  $R$  [31].

$$R(\phi) = \sqrt{(x_a - R_x \cos\phi)^2 + (y_a - R_x \sin\phi)^2} \quad (2)$$

Equation (2) defines the Euclidean distance between the actual position of the antenna and the positions of the scatterers for the specific angle. In Equation (2), the antenna position is denoted by  $(x_a, y_a)$ , and the angular distance of the scatterer from the center  $(0, 0)$  is denoted by  $(R_x, \phi)$ . The  $x$  index equal to  $t$  in the case of tumor scatterers and  $s$  in the case of skin scatterers. The  $v$  parameter given in Equation (1), which represents the speed of an electromagnetic wave inside a dielectric medium, is defined as in Equation (3) [9].

$$v = \begin{cases} c & \text{vacuum} \\ \frac{c}{\sqrt{\epsilon_r}} & \text{in a medium} \end{cases} \quad (3)$$

While an electromagnetic wave propagates with the speed of light ( $c$ ) in a vacuum, it travels at a slower speed in a dielectric medium. For the sake of simplicity, the environment covering the numerical model is considered to be a homogeneous vacuum medium. Equation (1) can be rearranged as given in Equation (4) using these assumptions [9].

$$\mathbf{E}_s(f, \phi) = \sum_{i=1}^n A_i e^{-j\left(\frac{4\pi f}{c}\right)R_i(\phi)} \quad (4)$$

$M$  and  $R_i$  are the numbers of scatterers in the imaging area and the Euclidean distance between the antenna and the scatterers, respectively, in Equation (4). The frequency-domain calculations were performed using stepped frequency continuous wave (SFCW). Each frequency sweep in SFCW was handled by  $N$  frequencies ( $f_1, f_2, f_3, \dots, f_N$ ). Thus, using Equation (4), scattered electric field data ( $\mathbf{E}_s[f, \phi]$ ) was obtained for all scatterers. The fundamental parameters and values utilized to compute the data are listed in Table 1.

**Table 1.** Variables and values for the computation of the scattered electrical field

Variable	Quantity
Lower Frequency	1 GHz
Upper Frequency	64 GHz
Number of Frequencies ( $N$ )	128
Center of the Imaging Plane ( $r, \phi$ )	$(0, 0^\circ)$
Radius of the Skin ( $r_s$ )	7 cm
space Between Skin and Antenna ( $D_{GAP}$ )	2 cm
Angle Increment Step	$1^\circ$
Number of Scatterer for Skin ( $n_s$ )	360
Number of Scatterer for Tumor ( $n_t$ )	360
Radius of the Tumor ( $r_t$ )	1 mm
Number of Scenarios	10001
Tumor Position ( $R, \phi$ )	$0 \leq r_t < r_s,$ $0 \leq \phi \leq 2\pi$
Number of Tumors	1 – 5
Amplitudes for Tumor Scatterers (V/m)	0 – 0.05

The scattered electric field data at various positions, amplitudes, and tumor count were computed based on the SAR approach using the values in Table 1. As shown in Table 1, the data set was collected using an SFCW with 128 frequencies between 1 GHz to 64 GHz. The range resolution for theoretical data was computed using Equation (5) by considering the frequency range [31].

$$\Delta r = \frac{c}{2B} \quad (5)$$

The range resolution, which is a measure of the distinctness between the two scatterers, was calculated to be 2.4 mm using Equation (5). Thus, each discrete step of the signal converted from the frequency domain to the time domain indicates the distance of 2.4 mm, and since the computations are performed for 128 frequency steps, the resulting data provide information on the area in the range of 30.72 cm. Due to the fact that the area outside the breast model is irrelevant, only 61 data containing information about the imaging area were extracted from the data. As a result, the dimensions of the electric field data matrix  $\mathbf{E}_s$  were obtained as  $61 \times 360$ .

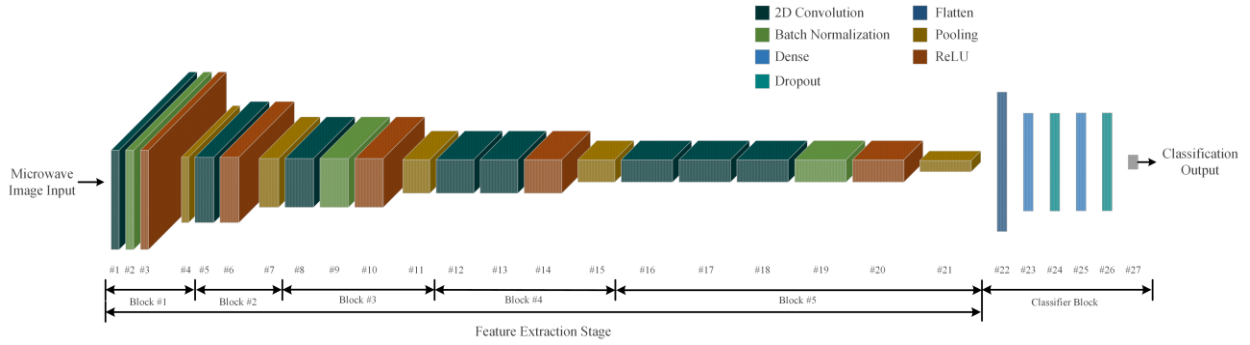


**Figure 2.** The proposed CNN-based classifier model

### 3. CLASSIFICATION OF SCATTERED ELECTRIC FIELD DATA

Convolutional neural networks (CNNs) are the most extensively used classification and regression networks in deep learning, particularly for two-dimensional data such as images and videos. The deep learning concept has gained the attention of researchers studying in the machine learning field. Deep learning models extract the features of the data in the network, allowing for direct utilization of the raw data. In this study, a CNN model is constructed for estimating the number of tumors using the scattered electric field data. The data for the complex backscattered electric field obtained using numerical models are  $61 \times 360$  cells in size. Both the amplitudes and angles of the scattered electric field data contain information about the electromagnetic properties of the numerical breast model. Due to the fact that the input data of the proposed CNN model were presented as images,

only amplitude information was employed to generate images. The generated images, which were composed of the amplitude of the  $61 \times 360$  data, were resized to  $100 \times 100$  pixels to be used in the proposed model.

Table 2 presents details of the layers of the proposed model denoted by the numbers between #1 and #27 in Figure 2. As shown in Table 2, the proposed model is composed of five convolutional blocks that serve as feature extractors and a classifier. The initial convolution block of the proposed model reduces redundant data while extracting the features of the  $100 \times 100$  image used as the input. To maintain optimal performance during training and testing, the kernel sizes in all convolution layers were set to be  $3 \times 3$ , and maximum pooling layers were employed. In blocks #4 and #5, it is aimed to obtain more features by increasing the number of convolution layers and their depth. To avoid overfitting, batch normalization was utilized in the convolution blocks #1,

**Table 2.** Detailed information about the layers of the proposed model

#	Blocks	Layer	Output Shape	Additional Properties	Parameters
1	Convolution Block #1	Depthwise Separable 2D Convolution Layer	100, 100, 16	Filter Size: $3 \times 3$	91
2		Batch Normalization Layer	100, 100, 16		64
3		Rectified Linear Unit Activation Layer	100, 100, 16		0
4		Maximum 2D Pooling Layer	50, 50, 16	Pool Size: $2 \times 2$	0
5	Convolution Block #2	Depthwise Separable 2D Convolution Layer	50, 50, 32	Filter Size: $3 \times 3$	688
6		Rectified Linear Unit Activation Layer	50, 50, 32		0
7		Maximum 2D Pooling Layer	25, 25, 32	Pool Size: $2 \times 2$	0
8	Convolution Block #3	Depthwise Separable 2D Convolution Layer	25, 25, 64	Filter Size: $3 \times 3$	2400
9		Batch Normalization Layer	25, 25, 64		256
10		Rectified Linear Unit Activation Layer	25, 25, 64		0
11		Maximum 2D Pooling Layer	12, 12, 64	Pool Size: $2 \times 2$	0
12	Convolution Block #4	Depthwise Separable 2D Convolution Layer	12, 12, 128	Filter Size: $3 \times 3$	8896
13		Depthwise Separable 2D Convolution Layer	12, 12, 128	Filter Size: $3 \times 3$	17664
14		Rectified Linear Unit Activation Layer	12, 12, 128		0
15	Convolution Block #5	Maximum 2D Pooling Layer Layer	11, 11, 128	Pool Size: $2 \times 2$ , Stride: $1 \times 1$	0
16		Depthwise Separable 2D Convolution Layer	11, 11, 256	Filter Size: $3 \times 3$	34176
17		Depthwise Separable 2D Convolution Layer	11, 11, 256	Filter Size: $3 \times 3$	68096
18		Depthwise Separable 2D Convolution Layer	11, 11, 256	Filter Size: $3 \times 3$	68096
19		Batch Normalization Layer	11, 11, 256		1024
20	Classifier Block	Rectified Linear Unit Activation Layer	11, 11, 256		0
21		Maximum 2D Pooling Layer	5, 5, 256	Pool Size: $2 \times 2$	0
22		Flatten Layer	6400		0
23		Fully Connected Layer	2048		13109248
24		Dropout Layer	2048	Dropout Rate: 0.25	0
25		Fully Connected Layer	2048		4196352
26	Dropout Layer	2048	Dropout Rate: 0.25	0	
27	Output Layer	5	Activation: SoftMax	10245	

#3, and #5, while dropout layers were utilized in the classifier block between the dense layers. The variable *Number of Tumors* in Table 1 indicates the number of classes in the proposed model.

The *Adam* optimization approach with a learning rate of 0.001 and the *He uniform* weight initializer are used during the training phase. The network was trained using 8000 randomly chosen data points from a total of 10001, and the model was tested using the remaining data points. The data for each class were chosen to have equal proportions. The model was trained on an Nvidia RTX 2060 GPU. The training procedure was performed several times with randomly selected new training and test data until the desired level of training and test accuracy was achieved. To evaluate the performance of the developed model, Xception [28], ResNet152V2 [29] and DenseNet201 [30] models were utilized, with all models performing five-fold cross-validation. State-of-the-art models were trained utilizing pre-trained weights from the *ImageNet* [32] data set, as well as the data set collected in this study.

#### 4. RESULTS AND DISCUSSION

Equation (4) and the values in Table 1 were used to generate the backscattered electric field data for each class, and the amplitude information was scaled to 100×100 pixels for network training. Figure 3a-e illustrates randomly chosen images from the raw electric field data for one to five tumors.

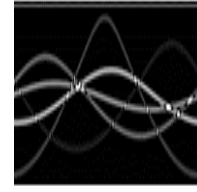
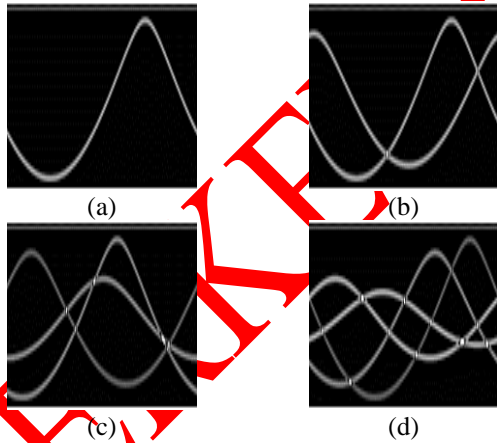


**Figure 3.** Raw data samples for (a) 1, (b) 2, (c) 3, (d) 4, and (e) 5 tumors in various positions

The proposed model was trained over 300 epochs using 8000 randomly selected data points, some of which are illustrated in Figure 3. The model achieved 99.61% and 99.75% accuracy for training and testing, respectively, resulting from the training. Figure 4a and Figure 4b show the categorical cross-entropy (CCE) loss and accuracy graphs for training and testing the model, respectively.

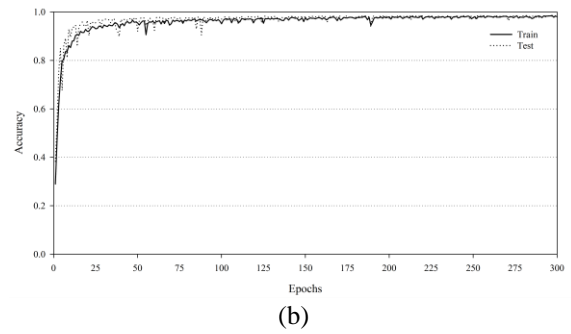
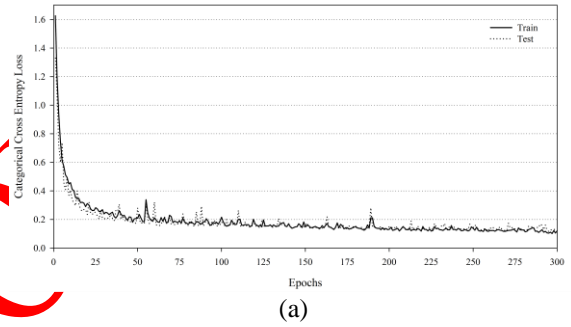


**Figure 4.** (a) Categorical cross-entropy loss and (b) accuracy curves for train and test process

As illustrated in Figure 4, there are peaks in both loss and accuracy curves at certain epochs.

**Table 3.** The performance measures of the proposed model for training and test data

Class	Precision		Recall		F1-score		Support	
	Train	Test	Train	Test	Train	Test	Train	Test
1	1.000	1.000	1.000	1.000	1.000	1.000	1616	404
2	0.997	1.000	1.000	1.000	0.998	1.000	1582	396
3	0.994	0.995	0.997	1.000	0.995	0.997	1522	381
4	0.991	0.993	0.995	0.995	0.993	0.994	1682	421
5	0.999	1.000	0.989	0.992	0.994	0.996	1598	399
<i>Average</i>	0.997	0.998	0.997	0.998	0.997	0.998	8000	2001

The model becomes trapped in a local minimum in the solution space at specific points yet continues to improve the findings by correcting its error in subsequent epochs. Over the 300 epochs, the model provided a generally steady evolution. The performance metrics of the proposed model for both training and test data are summarized in Table 3. The support column indicates the number of data points used to evaluate the model. As shown in Table 3, test data containing 1, 2, and 3 tumors were successfully classified. However, metrics for data with four and five classes were obtained at a lower level. Table 4 contains a confusion matrix table related to the classification of test data.

**Table 4.** Confusion matrix table obtained by the proposed model for test data

		Predicted Classes				
		1	2	3	4	5
Target Classes	1	404	0	0	0	0
	2	0	396	0	0	0
	3	0	0	381	0	0
	4	0	0	2	419	0
	5	0	0	0	3	396

As seen in Table 4, the network with a lower misclassification rate of up to three tumors may misclassify as the number of tumors increases. The table indicates that the proposed model made the highest classification errors in data with five tumors. The results indicate that the constructed neural model is quite effective at classifying microwave images of breast. To verify the success of the model, five-foldcross-validation

was performed on both the model and the state-of-the-art models. For five-foldcross validation, the epoch number and batch size were adjusted at 200 and 64, respectively. The cross-validation accuracies of the models are listed in Table 5. According to Table 5, state-of-the-art models have a lower accuracy when pre-trained weights are used, but a higher accuracy is obtained when all model weights are optimized utilizing the dataset. While the model proposed has the most accuracy in the third and fifth folds, the ResNet152V2 model achieves the most accuracy in the second and fourth folds, and the DenseNet201 model achieves the most accuracy in the first fold. On average, the proposed model achieved the highest accuracy for five-foldcross-validation. The cross-validation losses of the models are listed in Table 6. In terms of CCE loss values obtained from five-foldcross-validation, the proposed model has the lowest loss value in the second and fourth folds while Xception has the lowest loss value in the first and third folds, and DenseNet201 has the lowest loss value in the fourth fold. It is understood from the results that the accuracy value of the model with the lowest CCE loss value is not higher. However, the Xception model had the lowest loss value when pre-trained weights were used. Table 7 summarizes the time used by the models in each fold during five-foldcross-validation. As seen in the table, the proposed model required less training time than the state-of-the-art models. The difference between using pre-trained weights and optimizing entire weights was estimated to be between 2.6 and 3.4 times for the other models. Table 8 compares the number of parameters of the models used in this study.

**Table 5.** five-foldcross-validation accuracies of the proposed model, Xception, ResNet152V2 and DenseNet201

Fold #	Accuracy (%)							
	Our Model	Xception		ResNet152V2		DenseNet201		
		Pre-trained	Fully Trained	Pre-trained	Fully Trained	Pre-trained	Fully Trained	
1	98.70	84.76	98.90	85.81	98.55	91.20	<b>99.00</b>	
2	98.95	85.95	98.55	86.35	<b>99.05</b>	91.75	98.90	
3	<b>99.10</b>	84.60	98.95	86.05	99.00	91.15	98.80	
4	99.05	83.75	99.00	87.00	<b>99.15</b>	91.55	99.10	
5	<b>99.25</b>	84.70	98.85	85.55	98.90	90.65	99.05	
<i>Average</i>	<b>99.01±0.20</b>	86.75±4.55	98.85±0.18	86.15±0.56	98.93±0.23	91.26±0.42	98.97±0.12	

**Table 6.** five-foldcross-validation CCE losses of the proposed model, Xception, ResNet152V2 and DenseNet201

Fold #	Loss (Categorical Cross-Entropy (CCE))							
	Our Model	Xception		ResNet152V2		DenseNet201		
		Pre-trained	Fully Trained	Pre-trained	Fully Trained	Pre-trained	Fully Trained	
1	0.10	1.02	<b>0.09</b>	1.22	0.11	0.91	0.10	
2	<b>0.06</b>	1.10	0.10	1.53	<b>0.06</b>	0.92	0.07	
3	0.11	0.86	<b>0.06</b>	1.01	0.07	0.91	0.08	
4	<b>0.05</b>	1.04	0.08	1.12	0.08	0.92	0.06	
5	0.08	0.81	0.08	1.63	0.06	0.91	<b>0.05</b>	
<i>Average</i>	0.11±0.03	0.97±0.12	0.08±0.01	1.30±0.27	0.08±0.02	0.91±0.01	<b>0.07±0.02</b>	

**Table 7.** five-foldcross-validation durations of the proposed model, Xception, ResNet152V2 and DenseNet201

Fold #	Training Time (sec)						
	Our Model	Xception		ResNet152V2		DenseNet201	
		Pre-trained	Fully Trained	Pre-trained	Fully Trained	Pre-trained	Fully Trained
1	1596.85	1840.50	6277.41	4993.03	14092.49	3093.26	8262.26
2	1596.20	1835.15	6279.95	4846.27	14234.79	2871.76	9079.41
3	1580.99	1849.53	6206.04	4795.85	13912.86	2945.62	8883.86
4	1598.72	1857.19	6320.46	4800.95	13994.94	2941.37	8926.51
5	1598.91	1841.86	6340.98	4795.71	13794.65	2945.23	9196.00
<i>Average</i>	<b>1594.34±7.55</b>	1844.85±8.60	6284.97±51.74	4846.36±84.69	14005.95±168.29	2959.45±81.11	8869.60±361.55

**Table 8.** Parameter comparison of the proposed model, Xception, ResNet152V2 and DenseNet201

Model		Number of Trainable Parameters	Total Parameters
Our Model		17,516,624	17,517,296
Xception	with <i>ImageNet</i> Weights	18,880,517	39,741,997
	Fully Trained	20,817,197	20,871,725
ResNet152V2	with <i>ImageNet</i> Weights	33,560,581	91,892,229
	Fully Trained	58,198,149	58,341,893
DenseNet201	with <i>ImageNet</i> Weights	17,700,869	36,022,853
	Fully Trained	18,102,533	18,331,589

There are fewer parameters in the proposed model than in the other three models. The difference in the number of parameters between the pre-trained and fully trained structures in state-of-the-art models is due to the number of connections in the final layers of the models. As illustrated in Tables 5 and 8, a large number of parameters does not necessarily imply the best accuracy. It is demonstrated that the proposed model may be successfully applied to the classification of microwave imaging data.

## 6. CONCLUSION

In this study, a multi-layered CNN architecture was developed to be used along with the microwave imaging method in the detection of tumor formations, especially in breast cancer. The data set used to train the model was generated within the scope of this study using numerical breast models and theoretical equations. 8000 randomly chosen data points from a collection of 10001 numerically synthesized data points were used to train the model, and 2001 randomly chosen data points were used to test the model. As a result of the training, the training and test data were correctly classified by the ratios of 99.61% and 99.75%, respectively. Thus, tumor diagnosis using electromagnetic waves and artificial intelligence techniques would be possible with minimum injury to healthy tissues. This study proposes a methodology for computer-aided diagnostics to aid physicians and researchers in understanding microwave images. In future research, it may be feasible to classify tumor tissue and other breast tissues as tissues, and benign and malignant tumor tissues as tumors, utilizing microwave imaging data.

## DECLARATION OF ETHICAL STANDARDS

The author(s) of this article declare that the materials and methods used in this study do not require ethical committee permission and/or legal-special permission.

## AUTHORS' CONTRIBUTIONS

**Mustafa Berkan BIÇER:** Conceived and designed the analysis, collected the data, performed the analysis, wrote the manuscript.

**Uğur ELİİYİ:** Performed the analysis, wrote the manuscript.

**Deniz TÜRSEL ELİİYİ:** Performed the analysis, wrote the manuscript.

## CONFLICT OF INTEREST

There is no conflict of interest in this study.

## REFERENCES

- [1] Curado M. P., "Breast cancer in the world: incidence and mortality", *Salud Publica Mex.*, 53(5): 372–384, (2011).
- [2] Hassan A. M. and El-Shenawee M., "Review of electromagnetic techniques for breast cancer detection", *IEEE Rev. Biomed. Eng.*, 4: 103–118, (2011).
- [3] Nass S. J., Henderson I. C. and Lashof J. C., "*Mammography and Beyond: Developing Technologies for the Early Detection of Breast Cancer*", National Academy Press, (2002).
- [4] Fear E. C., Meaney P. M. and Stuchly M. A., "Microwaves for breast cancer detection?", *IEEE Potentials*, 22(1): 12, (2003).
- [5] Kurrant D., Sill J. and Fear E., "Tumor response estimation algorithm for radar-based microwave breast cancer", *Proceedings of the XXIXth URSI General Assembly*, Chicago, 6–9, (2015).
- [6] Winters D. W., Shea J. D., Kosmas P., Van Veen B. D. and Hagness S. C., "Three-dimensional microwave breast imaging: Dispersive dielectric properties estimation using patient-specific basis functions", *IEEE Transactions on Medical Imaging*, 28(7): 969–981, (2009).
- [7] Bindu G., Lonappan A., Thomas V., Aanandan C. K., Mathew K. T. and Abraham S. J., "Active microwave imaging for breast cancer detection", *Prog. Electromagn. Res.*, 58: 149–169, (2006).

- [8] Güren O., Çayören M., Ergene L. T. and Akduman I., "Surface impedance based microwave imaging method for breast cancer screening: Contrast-enhanced scenario", *Phys. Med. Biol.*, 59(19): 5725–5739, (2014).
- [9] Bicer M. B., Akdagli A. and Ozdemir C., "A matching-pursuit based approach for detecting and imaging breast cancer tumor", *Prog. Electromagn. Res. M*, 64: 65–76, (2018).
- [10] M Bicer. B. and Akdagli A., "Implementation of the inverse circular radon transform-based imaging approach for breast cancer screening", *Int. J. RF Microw. Comput. Eng.*, 28(6): e21279, (2018).
- [11] Bicer M. B. and Akdagli A., "An experimental study on microwave imaging of breast cancer with the use of tumor phantom", *Appl. Comput. Electromagn. Soc. J.*, 32(10): 941–947, (2017).
- [12] Davis S. K., Van Veen B. D., Hagness S. C. and Kelcz F., "Breast tumor characterization based on ultrawideband microwave backscatter", *IEEE Trans. Biomed. Eng.*, 55(1): 237–246, (2008).
- [13] Chen Y. and Kosmas P., "Detection and localization of tissue malignancy using contrast-enhanced microwave imaging: Exploring information theoretic criteria", *IEEE Trans. Biomed. Eng.*, 59(3): 766–776, (2012).
- [14] Xie Y., Guo B., Xu L., Li J. and Stoica P., "Multistatic adaptive microwave imaging for early breast cancer detection", *IEEE Trans. Biomed. Eng.*, 53(8): 1647–1657, (2006).
- [15] Fear E. C., Li X., Hagness S. C. and Stuchly M. A., "Confocal microwave imaging for breast cancer detection: Localization of tumors in three dimensions", *IEEE Trans. Biomed. Eng.*, 49(8): 812–822, (2002).
- [16] Klemm M., Craddock I., Leendertz J., Preece A. and Benjamin R., "Experimental and clinical results of breast cancer detection using UWB microwave radar", *IEEE International Symposium on Antennas and Propagation and USNC/URSI National Radio Science Meeting*, 1–4, (2008).
- [17] N Irishina., Moscoso M., and Dorn O., "Microwave imaging for early breast cancer detection using a shape-based strategy", *IEEE Trans. Biomed. Eng.*, 56(4): 1143–1153, (2009).
- [18] Lim H. B., Nung N. T. T., Li E. P. and Thang N. D., "Confocal microwave imaging for breast cancer detection: Delay-multiply-and-sum image reconstruction algorithm", *IEEE Transactions on Biomedical Engineering*, 55(6): 1697–1704, (2008).
- [19] Li X., Bond E. J., Van Veen B. D. and Hagness S. C., "An overview of ultra-wideband microwave imaging via space-time beamforming for early-stage breast-cancer detection", *IEEE Antennas Propag. Mag.*, 47(1): 19–34, (2005).
- [20] Nawel Z., Nabiha A., Nilanjan D. and Mokhtar S., "Adaptive semi supervised support vector machine semi supervised learning with features cooperation for breast cancer classification", *J. Med. Imaging Heal. Informatics*, 6(1): 53–62, (2016).
- [21] Tan M., Pu J. and Zheng B., "Optimization of breast mass classification using sequential forward floating selection (SFFS) and a support vector machine (SVM) model", *Int. J. Comput. Assist. Radiol. Surg.*, 9(6): 1005–1020, (2014).
- [22] Al-Hadidi M. R. A., Al-Gawagzeh M. Y. and Alsaaidah B. A., "Solving mammography problems of breast cancer detection using: Artificial neural networks and image processing techniques", *Indian J. Sci. Technol.*, 5(4): 2520–2528, (2012).
- [23] Yin J., Yang J. and Jiang Z., "Classification of breast mass lesions on dynamic contrast-enhanced magnetic resonance imaging by a computer-assisted diagnosis system based on quantitative analysis", *Oncol. Lett.*, 17(3): 2623–2630, (2019).
- [24] Woitek R., Spick C., Schernthaner M., Rudas M., Kapetas P., Bernathova M., Furtner J., Pinker K., Helbich T. H. and Balzter P. A. T., "A simple classification system (the Tree flowchart) for breast MRI can reduce the number of unnecessary biopsies in MRI-only lesions", *Eur. Radiol.*, 27(9): 3799–3809, (2017).
- [25] Abdel-Nasser M., Melendez J., Moreno A., Omer O. A. and Puig D., "Breast tumor classification in ultrasound images using texture analysis and super-resolution methods", *Eng. Appl. Artif. Intell.*, 59: 84–92, (2017).
- [26] Klimonda Z., Karwat P., Dobruch-Sobczak K., Piotrkowska-Wróblewska H. and Litniewski J., "Breast-lesions characterization using Quantitative Ultrasound features of peritumoral tissue", *Sci. Rep.*, 9(1): 1–9, (2019).
- [27] Conceição R. C., O'Halloran M., Glavin M. and Jones E., "Support vector machines for the classification of early-stage breast cancer based on radar target signatures", *Prog. Electromagn. Res. B*, 23: 311–327, (2010).
- [28] Chollet F., "Xception: Deep learning with depthwise separable convolutions", *Proceedings - 30th IEEE Conference on Computer Vision and Pattern Recognition*, (2017).
- [29] He K., Zhang X., Ren S. and Sun J., "Identity mappings in deep residual networks", *Lecture Notes in Computer Science (including subseries Lecture Notes in Artificial Intelligence and Lecture Notes in Bioinformatics)*, 9908, (2016).
- [30] Huang G., Liu Z., Van Der Maaten L. and Weinberger K. Q., "Densely connected convolutional networks", *Proceedings - 30th IEEE Conference on Computer Vision and Pattern Recognition*, (2017).
- [31] Özdemir C., "Inverse Synthetic Aperture Radar Imaging with MATLAB Algorithms", Wiley-Interscience, (2012).
- [32] Deng J., Dong W., Socher R., Li L.-J., Li K. and Fei-Fei L., "ImageNet: A large-scale hierarchical image database", (2010).